Journal of Engineering and Sustainable Development
Vol. 30, No. 02, March 2026
https://jeasd.uomustansiriyah.edu.iq/index.php/jeasd
ISSN 2520-0917
Research Article
https://doi.org/10.31272/jeasd.3259

Structural Fragility Behavior of Steel Lattice Power Transmission Tower Subjected to High-Intensity Wind Loading

Husain Khalaf Jarallah[1*], Hayder Ali Abbas[2]

[1]Department of Civil Engineering, Mustansiriyah University, Baghdad, Iraq.
[2]Department of Civil Engineering, Indian Institute of Technology-Madras, India.

[*]Email: khalfdce@uomustansiriyah.edu.iq

Article Info

Received	**04/02/2025**
Revised	**09/02/2026**
Accepted	**12/02/2026**

Abstract

Transmission towers are indeed vital components of power transmission lines, but they also belong to the category of complex structural systems. The ultimate strength of this system can be highly compromised by strong wind forces that may act on it, and thus allow a situation where there is an outage in the event of storms. This paper presents a case study assessment for a steel lattice high-voltage transmission tower located within Iraq's territory after experiencing extreme-intensity wind loads (tornado). An inelastic dynamic analysis was carried out to establish the effects of tornado wind loads on such types of structures. Two different approaches were adopted by this research; one based on performance per scaled full-scale model applying various independent intensities' loadings, while the other used a constant, systematically scaled set of records representing different levels of intensities. A cross-validation methodology was used to acquire the dynamic stability of the lattice tower. The results showed that this high-intensity wind speed is greater than the minimum design loads of the latest development code for structures in this area. There is an urgent need to check on those transmission towers located within highly risky areas, as emphasized by this study.

Keywords: Fragility curves, Nonlinear hinge properties, Performance-based wind design, Steel lattice tower, Time history analysis, Wind velocity.

1. Introduction

Lattice towers remain the most appropriate option for power line systems due to a mixture of factors involving their lightweight design, optimum material consumption, and quick manufacturing and erection processes. The steel lattice towers have main legs made from steel angles- a very common structural shape- with bracing members added [1]. These are among the best-modeled structures in structural engineering since keen modeling transmits analysis results effectively; hence, it is considered an advanced structure. Serious damages that may result from the transmission line if wrong modeling assumptions are used on service load levels can greatly enhance its failure possibility [2]. A transmission tower could collapse because of many reasons, such as wrong design assumptions, poor detailing, improper fabrication, variations, bolt grade, etc. [3]. The investigation required for structural capacity with integrity under different loading scenarios, particularly tornado effects, should be considered by structural designers. High-Intensity Winds (HIWs) are defined as positional movements with thermal stresses, which frequently occur in squall lines. The path of HIWs is normally narrow, and the forward velocity of the winds is much greater than that found with broad-front systems. Tornadoes produce three components: axial, radial, and tangential about the axis. Because of this complexity, it becomes important to define the effect of wind forces on a transmission line by considering tornado center positions relative to a transmission line system layout. The tornadoes are responsible for about 80% tower collapses. They also frequently lead to power outages [4]. In the United States, strong winds damaged a major 500 kV transmission tower in 1982, resulting in widespread power loss. In Canada and Colombia, more than 17 states experienced power outages in 2012 due to high wind velocities that caused lines to break and towers to fall [5]. In Turkey, 225 tornadoes have been reported in the last five years, which is more than half the total number experienced over the previous two centuries. This increase has been linked to the effects of climate change [6]. Structures are usually designed to withstand low winds and light ice; hence,

they may not be able to endure high-intensity winds (HIW). From an economic perspective, it is also impractical to design a transmission tower that can resist all tornadoes [7]. During field investigations of structures damaged by tornadoes, researchers noted shear failures within the body of 4-leg towers and possible shear failures at the ends of the masts, which contributed to the collapses [8]. Many researchers have studied the behavior of steel lattice towers. Abdulaqder et al. [1] investigated both linear and nonlinear analyses for steel lattice towers with various bracing systems using tower software. The analyzed towers were constructed using beam elements to represent the main sections, while the bracing employed truss members. Results showed there is no difference between linear and non-linear analysis for towers less than 50 m in height. Gamal et al. [9] assessed two transmission towers under wind loads using Incremental Dynamic Analysis (IDA) and Nonlinear Static Analysis(NSA). They compared the capacity curves obtained from both analysis methods. There was no significant difference between the two curves. Nezamolmolki and Shooshtari [2] studied the effect of nonlinear modeling of joint slippage on the dynamic behavior of a lattice tower subjected to wind and earthquake loads. The study highlighted that accounting for joint slippage affects natural frequencies of the towers, resulting in a steady decrease in natural frequency when slippage is accounted for. Mahmoud et al. [10] evaluated 81 towers that failed in Egypt due to high wind velocities of more than 200 km/h. Their study used incremental dynamic analysis considering material and geometrical nonlinearity. The results also indicated that there is no difference between actual failure modes and those of finite element (FE) models for the type of towers studied. Salaamet al [11] studied the combined wind and dust load effect on the failure of transmission towers. Their results show that an increase in 0.01% of dust particles present in the air increases wind pressure by about 10%. Zhang et al [12] carried out a study on the effects of wind pressure at different yaw angles towards a transmission tower, wherein four different directions with several time histories were considered; random effects due to yielding stage members have been observed after which it fails under varying modes corresponding to different yaw angles of applied loads (wind). Fu and Li [13] found that high rain load intensity can cause large displacement. The study concluded that rain loads should not be ignored since they have a considerable effect on the dynamic properties of tower structures.

This study applies two different methods in the determination of tornado wind speeds. One is Performance-Based Wind Design (PBWD), and the other method happens to be what has been variously referred to as Performance-Based Fragility Design/Analysis/(PBFD)/(PBFA) in literature. The PBFA acts both as a cross-checking tool and a cumulative strength degradation assessment approach since that kind of fragility-based analysis adequately reflects how much cumulative damage influences progressive structural capacity loss, specifically for transmission towers under consideration here. IDA was used so that full structural response could be evaluated starting from elastic behavior up to dynamic instability initiation at different levels or intensities of wind loading on the structure being analyzed; though normally applied with respect to earthquake-excited structures only, However, note well that, unlike seismic loading which is a zero-mean stochastic effect, the wind velocity drag force can be represented as a non-zero mean load due to the mean wind velocity and fluctuating stochastic excitations [9].

2. Significance of Research

The most significant point of this research is:

1. To develop a method that uses Fast Fourier Transform (FFT) to convert wind velocity into frequency to check the resonance effect on transmission tower failures.

2. To check a finite element model of the transmission tower by using inelastic dynamic time history analysis. It computes the probability of failure by using inelastic element sections that consider geometric and material nonlinearity.

3. To validate the *Performance-Based Wind Design (PBWD)*, damage assessment is carried out based on the acceptance criteria for plastic hinges in the primary beam and bracing elements. The evaluation is methodologically cross-verified with the *Performance-Based Fragility Design (PBFD)*. Accordingly, cumulative damage is quantified and validated through four complementary failure criteria: (a) deformation-based, (b) strength-based, (c) performance-based, and (d) fragility-based approaches**.**

3. Method of the Research

3.1. Codal Provisions

The primary lateral loads considered in structural design are wind and earthquake forces. Most wind design codes focus solely on the elastic response of structures, whereas seismic design codes also incorporate inelastic behavior. Wind effects can exceed seismic loads [14]. This study will summarize the ASCE-74 [7] guidelines, which outline the concepts of wind loading for transmission towers.

3.2. Transmission Line Structural Loading Guidelines

3.2.1. Calculation of the Wind Loading

The effects of weather on transmission structures are covered in this paragraph. These are the loads carried by the wind, the ice, or both wind and ice. Equation (1) is used to calculate the wind forces applied to the transmission line.

$$F = \gamma_{\mathrm{w}} Q K_{\mathrm{z}} K_{\mathrm{zt}} (V_{50})^2 G C_{\mathrm{f}} A \quad (1)$$

where;

F is the wind force in the wind's direction, γ_{w} is the value to adjust the wind loads to the appropriate return periods, Q is the factor equal to 0.613 in metric units, K_{z} It is calculated based on (2), taking into account the velocity factor of the pressure exposure.

$$K_{\mathrm{z}} = 2.01 \left(\frac{z_{\mathrm{h}}}{z_{\mathrm{g}}}\right)^{\frac{2}{\alpha}} \text{ for } 33 \leq \mathrm{z_h} \leq \mathrm{z_g} \quad (2)$$

Theoretically, z_h represents the effective height from the above ground to the center of the wind load pressure, $z_g$is the gradient height, and α is the power law exponent. The values of α and Z_g based on exposure category and the possibility to calculate K_z based on Z_h are provided in ASCE-74 [7].

K_{zt} It is the topographic factor, calculated as per (3)

$$K_{zt} = (1 + K_1K_2K_3)^2 \quad (3)$$

ASCE 7-22 [15] assumes that the value of K_{zt} should be at least 1.0.

V_{50} is basic wind velocity, 50-year return period, 3-sec gust, in mph (m/h).

G is the gust response factor. There are two equations to determine the factor of the gust response: one for the ground wires and conductors, and the other for the structures.

$$G_w = \frac{1+2.7E\sqrt{B_w}}{K_v 2} \quad (4)$$

$$G_t = \frac{1+2.7E\sqrt{B_t}}{K_v 2} \quad (5)$$

In which,

$$E = 4.9\sqrt{\kappa}\left(\frac{33}{z_h}\right)^{\frac{1}{\alpha FM}} \quad (6)$$

$$B_w = \frac{1}{1+\frac{0.8S}{L_s}} \quad (7)$$

$$B_t = \frac{1}{1+\frac{0.56z_h}{L_s}} \quad (8)$$

Where,

z_h represents a factor equal to 2/3 of the overall structure to specify G_t, K_v is equal to 1.43, S is the design distance of the conductors and ground wires, αFM, κ, and Ls are factors provided in ASCE-74 [7].

C_f is the drag coefficient, it is the function of the solidity ratio, φ, defined as (9):

$$\Phi = \frac{A_m}{A_o} \quad (9)$$

Where A_m expresses to the area of all members in the direction of the windward face and A_o is the transverse area in the direction of the structure windward.

3.2.2. Wind Loading at Yawed Angle Calculation

For yawed wind forces, the ASCE standard determines the loads on the tower in the transverse and longitudinal axes separately by applying the following:

$$F_t = \gamma_w Q K_z K_{zt} V^2 G_t \cos\Psi C_{ft} A_{mt} \quad (10)$$

$$F_1 = \gamma_w Q K_z K_{zt} V^2 G_t \sin\Psi C_{fl} A_{ml} \quad (11)$$

Where, F_t and F_1 considers the transverse and longitudinal forces, respectively, Ψ is the yaw angle, C_{ft} and C_{fl} are the drag coefficients and A_{mt} and A_{ml} the member's area in the direction under consideration.

3.2.3. High Intensity Winds (HIW) Calculation

One of the HIW phenomena that can be found in the majority of the world's temperate and subtropical landmasses is the tornado.

Fujita and Pearson [16] developed a scale named FPP to calculate the tornadoes within the size and the level of severity. This scale is related to the width, length, and velocity of the wind, as illustrated in ASCE-74 [7]. This methodology gives a value for each tornado. ASCE depends on the tornadoes, which have a wind velocity of 157 mph and are represented on the F2 scale. ASCE assumes that no forces are applied to the wires of the towers. Additionally, three loading cases should be calculated with tornado effects: 0 °, 90 °, and 45 ° yaw angles.

These procedures are used in the design processes for the transmission tower's structure. For *Performance-Based Wind Design (PBWD)* and since the codes focus on static methods, probably, in order to model the wind velocity history, which is equal to the component of the wind turbulence, in addition to the average wind velocity. Fig. 1 depicts the state of the wind loads calculation.

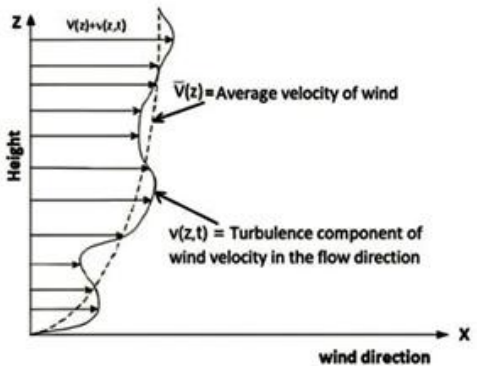

Figure 1. Wind velocity variations versus height [17].

The average wind velocity and turbulence will be separated into two categories for each desired level.

$$V(z,t) = \bar{V}(z) + v(z,t) \quad (12)$$

where V (z, t) represents the function of the wind velocity with variable level (z) and time (t), $\bar{V}(z)$ represents an average velocity of the wind at (z) level, and v (z, t) delineates the profile of the wind turbulence at (z) level and (t) time. Equations (13), (14), (15), and (16) provide the information to calculate the force history applied at each level of the tower, considering the combined average wind velocity and turbulence profile [16].

$$p_z = q_z G_f C_p \quad (13)$$

$$F = 0.613 K_z K_{zt} (V_{50})^2 G C_f \quad (14)$$

$$V(t, z = 10m) = \bar{V}(z = 10) + V(t) \quad (15)$$

and

$$\bar{V}(z = 10) = \bar{b} \times V^{\bar{b}=0.45} = 0.45\text{V} \quad (16)$$

Each level of the structure experiences dynamic loads, and the analysis method can be performed using any finite element (FE) software based on the developed time history function [17].

It is important to distinguish between the two primary types of damping relevant to lattice tower structures: aerodynamic damping and structural damping. Aerodynamic damping arises from the presence of wires and conductors; however, even though this form of damping was not explicitly modeled in the present study, the analysis incorporated the effects of cables and conductor self-weights as axial forces applied to designated nodes within the structure under wind loading conditions. Regarding structural damping, it is inherently accounted for through the gust response factor, consistent with Equation F2 of ASCE 74 [7] and (5) above. In this study, the gust response factor was conservatively assumed to be unity in the computation of wind loads, in accordance with (16) above, given that tornado wind speeds are inherently considered as gust wind speeds as per ASCE 74[7]. Additionally, Rayleigh damping was implemented in the OpenSees to model the inherent structural damping behavior of the lattice tower system.

3.3. AL-Kahala Tornado 2016 Descriptions

The tornado incident occurred in the northern part of Al-Kahlaa, specifically at the coordinates (47° E, 31° N), approximately 20 kilometers south of Amarah city in the Missan governorate, Iraq, around 13:30 local time on April 14, 2016. The town has a population that could total up to 85000 people. The area surrounding the town's center features flat terrain, primarily consisting of agricultural land. The houses in this region are no taller than 10 meters. Fig. 2 illustrates the approximate location of the tornado [18].

Figure 2. The approximate location of the tornado [18].

Fig. 3 illustrates the extent of the damage inflicted by the Al-Kahlaa tornado on the northern side of Al-Kahlaa town. Despite the significant destruction of multiple tall power transmission towers, residential structures, and vehicles, no injuries were reported. Additionally, a secondary funnel vortex was observed within the cloud formation; however, it did not make ground contact.

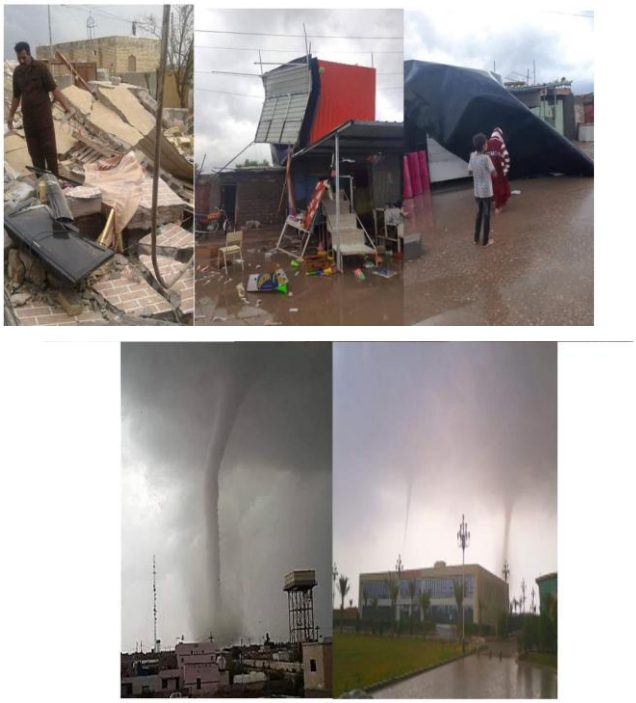

Figure 3. The damage on the path of the tornado [18].

3.4. Tornado-Induced Tower Failure

The current study investigates the failure of an existing lattice transmission tower caused by the Al-Kahala tornado in 2016. The tower, a suspension type known as “S-2S + 3BODY,” is designed with a height of 15 meters. Fig. 4 illustrates the condition of the tower after it was exposed to the Al-Kahala tornado in 2016.

Figure 4. The case of the tower under study after a tornado.

3.5. Structural Configuration of the Transmission Tower

Design loads for towers are described by climatic conditions (a combination of wind, ice, and temperature), load factors, and conductor. All loads applied to the tower are computed. These loads are arranged in load combinations and given in Table 1. Fig. 5 shows the 33 kV double circuit transmission lines “S-2S” Type suspension tower.

Table 1. Combination load cases.

System	Load Condition	Load Values	Wind pressure
Conductor	Vertical loads (+15 °C)	163 kg	94 kg/m^2
Conductor	Transverse loads (+15 °C)	370 kg	94 kg/m^2
Conductor	Transverse loads with the yawed wind of 45 degrees	195 kg	94 kg/m^2
Conductor	Transverse loads -5 ice)	434 kg	94 kg/m^2
Conductor	Vertical loads (+15°°C) with maximum wind	251 kg	94 kg/m^2
Conductor	Long loads	148 kg	94 kg/m^2
Conductor	Stringing and maintenance conditions	694 kg	94 kg/m^2

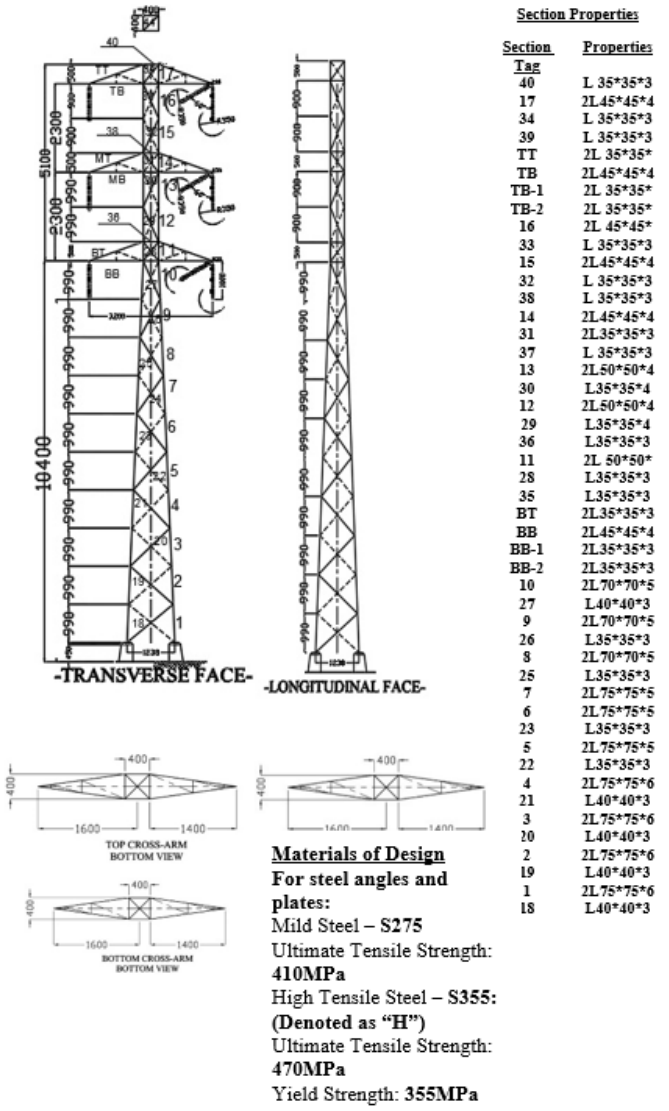

Section Properties

Section Tag	Properties
40	L 35*35*3
17	2L45*45*4
34	L 35*35*3
39	L 35*35*3
TT	2L 35*35*
TB	2L45*45*4
TB-1	2L 35*35*
TB-2	2L 35*35*
16	2L 45*45*
33	L 35*35*3
15	2L45*45*4
32	L 35*35*3
38	L 35*35*3
14	2L45*45*4
31	2L35*35*3
37	L 35*35*3
13	2L50*50*4
30	L35*35*4
12	2L50*50*4
29	L35*35*4
36	L35*35*3
11	2L 50*50*
28	L35*35*3
35	L35*35*3
BT	2L35*35*3
BB	2L45*45*4
BB-1	2L35*35*3
BB-2	2L35*35*3
10	2L70*70*5
27	L40*40*3
9	2L70*70*5
26	L35*35*3
8	2L70*70*5
25	L35*35*3
7	2L75*75*5
6	2L75*75*5
23	L35*35*3
5	2L75*75*5
22	L35*35*3
4	2L75*75*6
21	L40*40*3
3	2L75*75*6
20	L40*40*3
2	2L75*75*6
19	L40*40*3
1	2L75*75*6
18	L40*40*3

Figure 5. Tower structural configuration.

3.6. Time-History Modeling of Wind Velocity

The wind velocity profiles were analyzed in the days leading up to and following the tornado event. Fig. 6 illustrates the visualization of wind velocity during the tornado event [18]. In this study, the wind velocity time history was scaled until the tower failure occurred. The data were sourced from the Iraqi Meteorological and Seismology Organization and were collected in collaboration with the Department of Atmospheric Sciences at Mustansiriyah University, Iraq. Fig. 7 presents the time histories of wind velocity collected during the research.

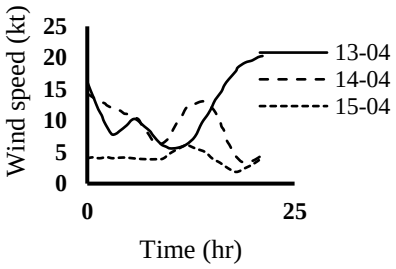

Figure 6. Wind velocity time history based on Missan city station knots (1 kt = 0.514 m/sec) [18].

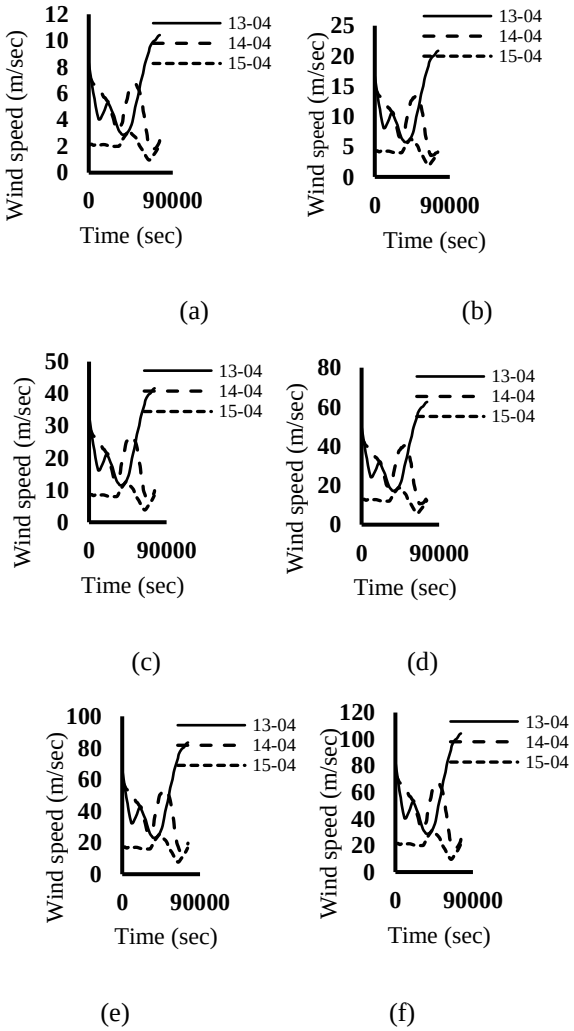

Figure 7. (a) Convert Kt to m/sec, (b) 2*Wind, (c) 4*W, (d) 6*W, (e) 8*W, and (f) 10*W, Wind velocity time history under study.

3.7. Analysis of Wind Velocity Time History

To calculate the frequency of the wind velocity, this section analyzes the time histories of the wind velocity. The objective of determining the wind excitation frequencies is to enable a comparative analysis with the natural frequencies of the transmission tower, using eigenvalue analysis, to identify potential resonance phenomena that may contribute to

structural failure. This assessment is performed through the application of the Fourier Transform, which facilitates the extraction of dominant frequency components from the wind-induced acceleration time histories, which are created in MATLAB/Simulink [19]. Equation (17) represents the expression of the Fast Fourier Transform (FFT):

$$A(f) = \sum a(t) \cdot e^{\wedge}(-i \cdot 2\pi \cdot f \cdot t) \qquad (17)$$

where;
A(f) = Fourier Transform of a(t), a(t) = Time-domain signal (wind velocity data), N = Total number of samples, f = Frequency in Hz, i Imaginary unit. Fig. 8 presents the flowchart to construct the frequency domain of the wind velocity.

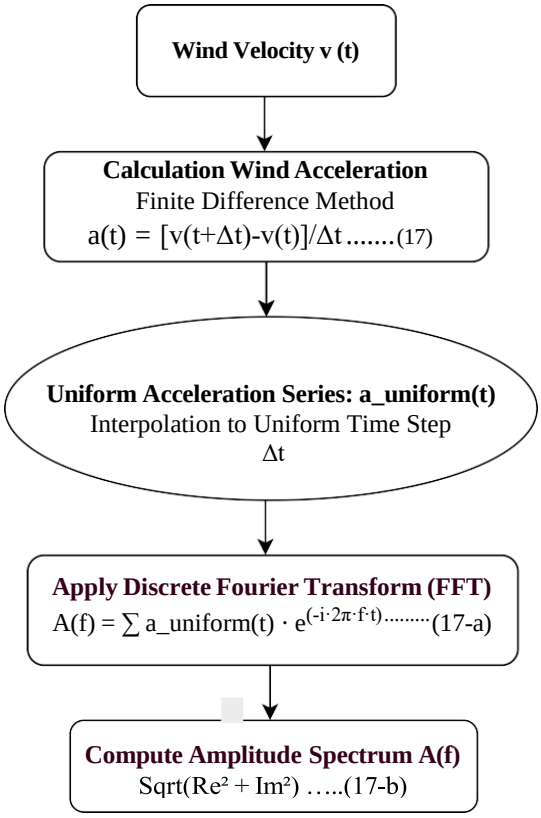

Figure 8. Flowchart illustrating the conversion of wind velocity to the frequency domain.

Fig. 9 reflects the process of converting the time history wind speed to frequency.

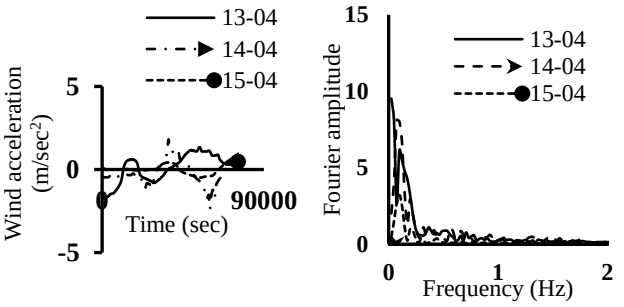

(a) Scale 2*Wind Velocity

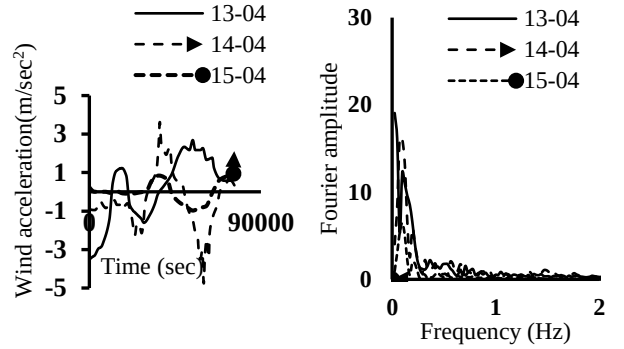

(b) Scale 4*Wind Velocity

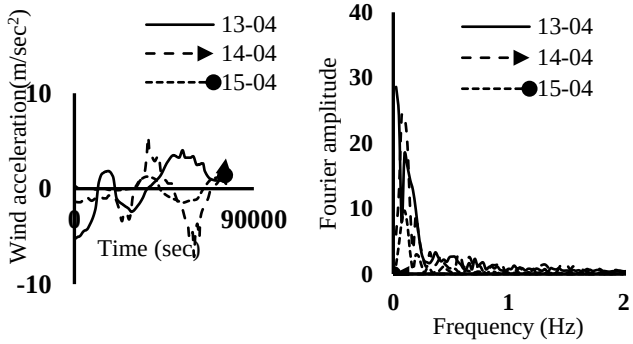

(c) Scale 6*Wind Velocity

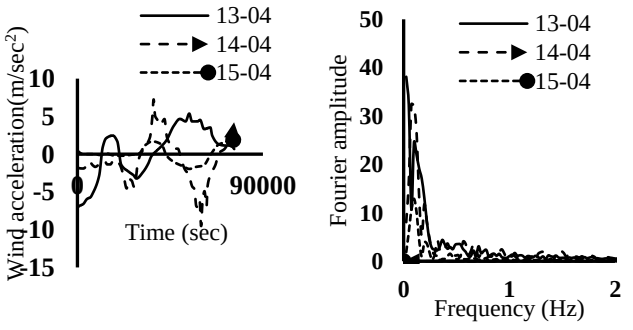

(d) Scale 8*Wind Velocity

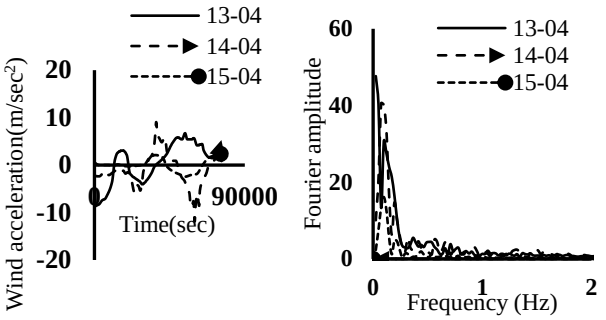

(e) Scale 10*Wind Velocity

Figure 9. Conversion of transforming the scaled wind velocity time history into the frequency domain.

3.8. Nonlinearity Modeling of the Lattice Tower

The material nonlinearity and geometric nonlinearity are recognized in this study for the lattice transmission tower.

3.8.1. Nonlinearity of the Materials

The nonlinearity of materials can be characterized using a nonlinear stress-strain relationship. In this study, two approaches were employed to analyze material nonlinearity: the plastic hinge approach using SAP2000 software [20] and the fiber section method using OpenSees [21]. In the fiber section method, sections are divided into refined meshes with regular shapes. The sections were discretized with a fiber model consisting of approximately 40 fibres. Based on the analysis conducted in OpenSees, discretizing the small-angle section into 40 fibers provided an adequate level of accuracy and convergence, making it sufficient for reliable results. The stress-strain relationships for each part are defined based on the specific constituent materials. Consequently, forces at the integration points are determined using data from the meshes, resulting in the calculation of forces at both ends of the elements. This nonlinearity in material behavior is achieved through the fiber section method. Fig. 10 illustrates the details of the component with the fiber section.

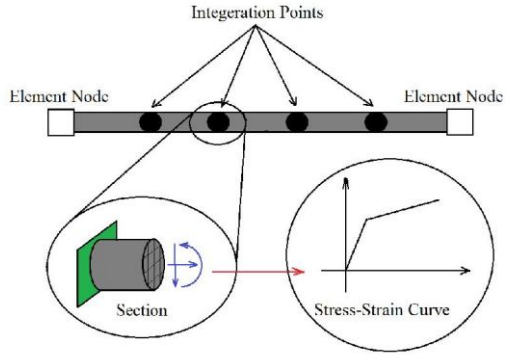

Figure 10. Element details with section fiber in OpenSees.

According to the uniaxial bilinear steel material, the stress-strain relationship of the steel section is established. Fig. 11 shows the stress-strain used in the OpenSees model.

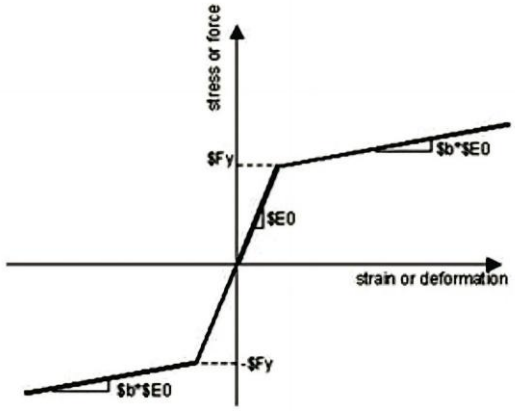

Figure 11. Stress-strain relation using (Steel01 Material) in OpenSees [21].

The material nonlinearity was implemented using the user-defined plastic hinges of the SAP2000 software environment. The tower sections were modeled and analyzed using beam-column and truss elements. The requirements are satisfied with the nonlinear dynamic analysis, the maximum plastic deformations are provided in ASCE-41 [22], which were implemented as user-defined for all sections of the lattice tower. Also, the acceptance criteria were defined according to the tables above. Fig. 12 reflects the relation between the moment-rotation of the steel elements.

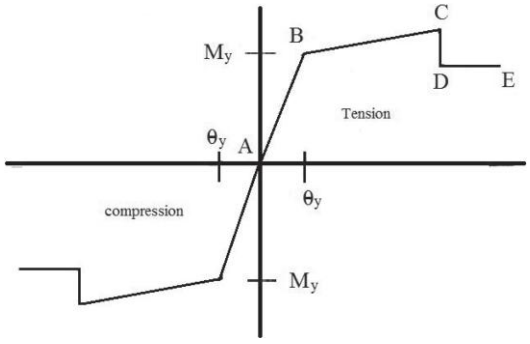

Figure 12. Moment-Rotation diagram for a moment hinge in steel members [17].

3.8.2. Geometric Nonlinearity

P-Delta effect (P-Δ) and the P-delta effect (P-δ) elaborate the geometric nonlinearity effects, which are considered the most crucial and taken into account in the nonlinear analysis, as shown in Fig. 13.

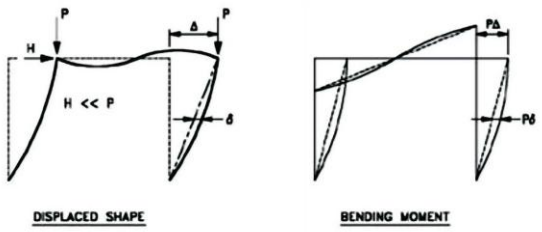

Figure 13. Geometric non-linear effects.

P-Δ occurs when loads are displaced due to deflections, producing additional bending moments that are not accounted for in linear analysis. The P-delta effect (P-δ) describes how axial compression reduces a member's bending stiffness while axial tension increases it [23].

4. Analysis Results and Discussions

4.1. Model Analysis of the Transmission Tower

The natural periods and frequencies of the current transmission tower are presented in Table 2, obtained using the OpenSees and SAP 2000 software.

Table 2. Transmission tower natural frequencies and periods.

Mode	OpenSees		SAP2000	
	Natural Period (sec)	Natural Frequency (rad/sec)	Natural Period (sec)	Natural Frequency (rad/sec)
1	0.255	24.6	0.233	26.9
2	0.243	25.9	0.218	28.7
3	0.158	39.7	0.158	39.8
4	0.0864	72.7	0.079	78.6

Analysis results emphasize the variation between the two approaches. The first model used fiber-section elements, which defined a nonlinear stress-strain relationship for each fiber (i.e., using "element nonlinear Beam Column" to define the elements in OpenSees), thus allowing a detailed representation at the material level. The natural periods have been lengthened because of the reduction in the effective stiffness of the sections. In the second approach, linear elastic frame elements were used with section and material properties specified (e.g., modulus of elasticity, shear modulus). However, this approach assumed fully elastic behavior across the entire section when computing stiffness [22].

Table 3 presents the natural frequency values for both the wind and the tower under investigation. The Fourier amplitude spectrum of the wind acceleration indicates that the dominant excitation frequencies are primarily concentrated between 0 and 2 Hz. In comparison, the natural frequencies of the transmission tower, obtained from model analysis of two approaches, begin at approximately 3.9 Hz. As a result, resonance is not anticipated. Thus, it is unlikely that the wind loading will excite the primary dynamic modes of the structure, and the study does not expect to observe any significant resonance effects.

Table 3. Verification of the resonant case.

Transmission tower Natural Frequencies (Hz)		Natural Frequencies of the wind time history (Hz)		Resonance Verification
OpenSees	SAP2000	Actual (max) 13-04	14-04	
3.915	4.281	1-2	1-2	No
4.122	4.567	1-2	1-2	No
6.318	6.334	1-2	1-2	No
11.570	12.509	1-2	1-2	No

4.2. Time History Analysis Subjected to Al-Kahala High Intensity Wind Loading

In this study, the methodology incorporating two components—average wind velocity and turbulence—was applied to each level of the tower structure, as illustrated in Fig. 2. Equations (16)-(20) were utilized for the current transmission tower. It is important to consider the function of wind time history in the dynamic analysis, even though high-intensity wind loading and failure containment were not included in the design considerations for the existing transmission tower. The relationship between pressure and velocity is discussed in terms of (18).

$$p_z = q_z G_f C_p \tag{18}$$

$$q_z = 0.613 K_z K_{zt} K_d V^2. \tag{19}$$

where K_d Supposes equal to 0.85, and it represents the directional coefficient, K_z It is a coefficient related to the topographic conditions around the structure and is presumed to be equal to the equation below.

$$q_z = 0.52105 K_z V^2$$

$$K_z = 2.01 \left(\frac{z_h}{z_g}\right)^{\frac{2}{\alpha}} = 0.61642 \text{ z } 0.21052$$

Where assuming C wind exposure category.

$$P_z = 0.321185\, Z^{0.21052}\, cp\, V^2$$

V represents the design wind velocity with z equal to 10m above the ground level. Equation 20 reflects the time function that was used in the study.

$$V(t, z = 10m) = \bar{V}(z = 10) + V(t) \tag{20}$$

and

$$\bar{V}(z = 10) = \bar{b} \times V^{\bar{b}=0.45} = 0.45\text{V}$$

The load function is performed on the tower joints at each level of the tower body based on (21):

$$P_z = 0.321185\, Z^{0.21052}\, cp[\bar{V}(z = 10) + V(t)]^2 \tag{21}$$

Fig. 14 shows the wind pressure history along the tower level as a biaxial effect in x and y directions, which is distributed on the level nodes.

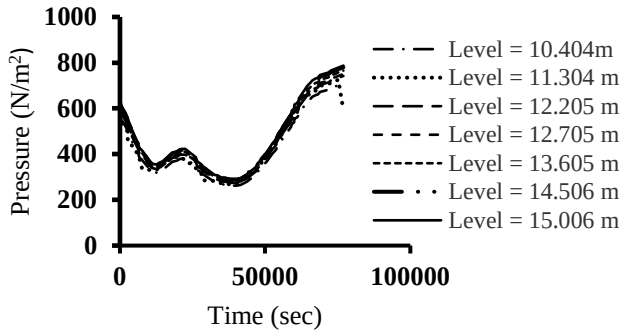

Figure 14. Relationship of pressure with time distribution along the tower.

4.3. Non-Linear Analysis Results and Discussions of Actual Wind Time History Loads

Two-time history analyses were conducted using the SAP2000 and OpenSees software. The performance level is determined by the formation of plastic hinges in the beam-column elements, and truss elements are provided in ASCE 41 [22] in the SAP2000 software. In the case of OpenSees, the performance level is based on fragility curves developed through incremental dynamic analysis (IDA), which are defined using drift limitations according to FEMA-350 [24] and have been used by others [25].

4.4. Estimating the Velocity of the Al-Kahala tornado 2016 according to the Performance Level

Using the SAP2000 software, the study estimated the velocity of the Al-Kahala tornado in 2016 based on its performance level. The wind velocity used in this study is illustrated in Fig. 7, which includes a scale for both wind velocity and the wind pressure applied to the lattice tower. Additionally, Fig. 15 displays the formation of plastic hinges in the (SAP2000) environment for the scales being studied.

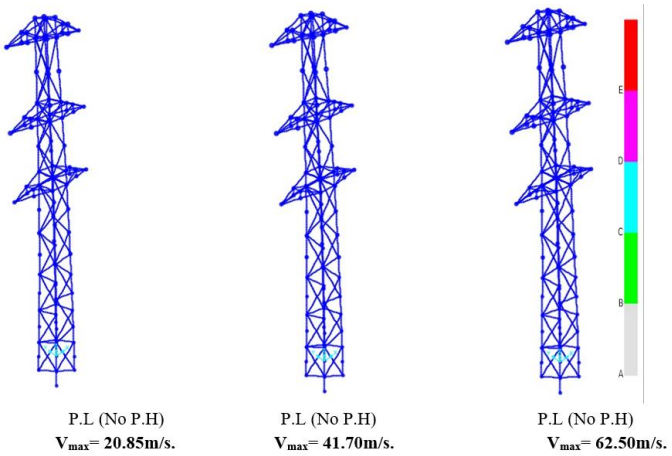

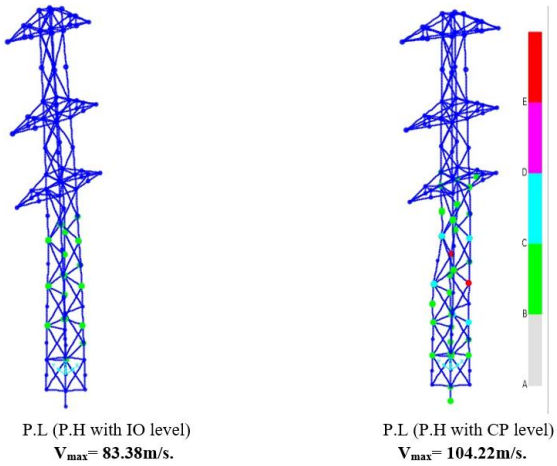

Figure 15. Plastic hinge formation of the lattice tower under scale wind load.

The results of the study reveal that the methodology employed to estimate the velocity of the high-intensity wind during the Al-Kahala Tornado in 2016 was highly accurate. The approach reflected the actual conditions that led to the failure of the existing lattice tower by monitoring the formation of plastic hinges in the structure due to concentrated dynamic forces acting on the nodes. A scale factor was also applied in the analysis. The existing steel tower is damaged at wind velocities ranging from 83.38 to 104.22 m/sec, which exceed the design wind velocity. This indicates that the wind risk zone in Missan City is subject to wind velocities greater than those specified in the recent design code for minimum design loads for buildings and other structures in Iraq. Table 4 presents the plastic hinge configurations of the tower under the scaled time-history wind pressure.

Table 4. Plastic Hinge Formation Values of the tower under Time History Wind Pressure

Type	A to IO	IO to LS	LS to CP	> CP
Scale (2*Wind velocity)	401	-	-	-
Scale (4*Wind velocity)	401	-	-	-
Scale (6*Wind velocity)	401	-	-	-
Scale (8*Wind velocity)	383	18	-	-
Scale (10*Wind velocity)	367	21	3	10

4.5. Results of Base Shear Histories

Fig. 16 illustrates the base shear histories of the models subjected to wind load time histories in the X-direction. The results indicate that the base shear for the model at scale 10 increased by approximately 50.12% compared to the model at scale 8, by about 180% compared to the model at scale 6, by about 262.83% compared to the model at scale 4, and by about 577.71% compared to the model at scale 2. This increase in base shear demonstrates the tower's enhanced ability to resist wind tornado pressure. Fig. 16 shows the base shear histories of the models under the wind load time histories in the Y-direction. From the results, the base shear of the model with scale 10 increased by about 61.18%, compared to the model with scale 8, by about 125.75%, compared to the model with scale 6, by about 272.28%, compared to the model with scale 4, and by

about 626.71% compared to the model with scale 2. The increasing percentage in the y-direction compared with the x-direction means that the tower in the y-direction has the most significant resistance against the wind tornado event. The effect of wind loads at principal orthogonal angles (0° and 90°). These directions correspond to maximum load effects on frames due to the alignment with the principal axes of stiffness and exposure.

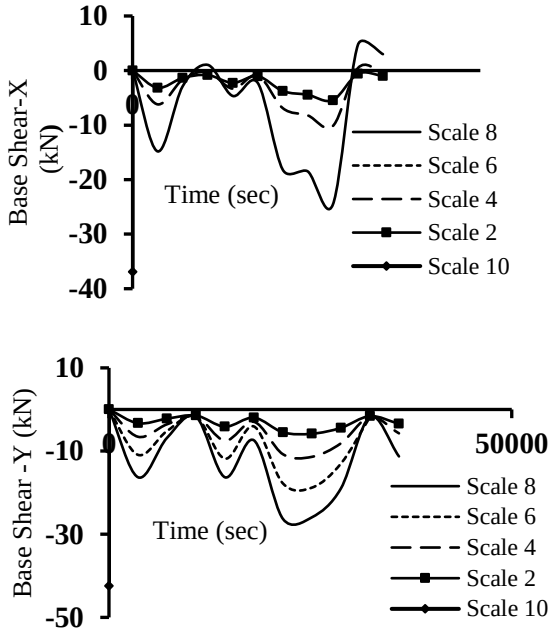

Figure 16. Base Shear Histories in X and Y-direction of the models under the scaled wind pressure.

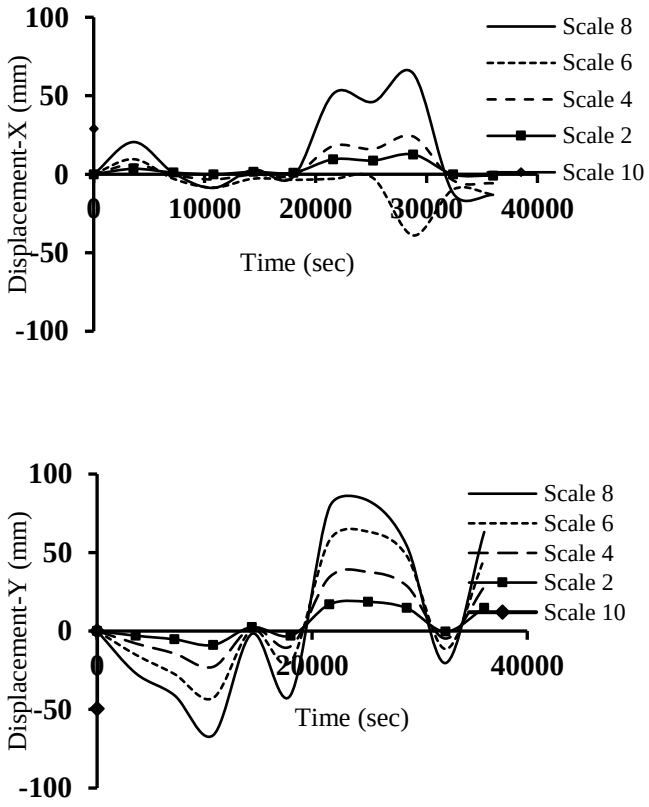

Figure 17. Displacement histories in the X and Y-direction of the models under the scaled wind pressure.

4.6. Results of Displacement Histories

Fig. 17a illustrates the displacement histories of the models subjected to wind load time histories in the x-direction. The results indicate that the tip displacement of the scale 10 model in the x-direction decreased by approximately 54.6% compared to the scale 8 model. In contrast, it increased by about 203.75% when compared to the scale 6 model, showed a reduction of about 21.09% relative to the scale 4 model, and increased by approximately 130.87% compared to the scale 2 model. This decrease in displacement for the scale 10 model can be attributed to the brittle behavior of the tower under dynamic wind tornado loads. Fig. 17 b presents the displacement histories of the models again under wind load time histories in the y-direction. The findings reveal that the tip displacement of the scale 10 model decreased by about 40.45% when compared to the scale 8 model, decreased by 21.82% compared to the scale 6 model, increased by 31.57% relative to the scale 4 model, and rose by approximately 165.85% when compared to the scale 2 model.

4.7. Estimating the velocity of the Al-Kahala tornado 2016 according to Incremental Dynamic Analysis

In this study, IDA analysis was employed to evaluate the lattice tower's capacity. IDA is considered a more creative tool for carrying out nonlinear analysis. It is used to determine the overall response of tower structures, ranging from elastic to dynamic instability, under wind dynamic loads. In this study, the IDA was adopted to evaluate the structural capacity under wind loading by developing a code and carrying out the analysis in the OpenSees environment.

4.7.1. Results of Top Tower Displacement

Fig. 18 illustrates the displacement time histories of the lattice tower under wind load records scaled using an intensity measure. The displacement values increased with the wind intensity measure, which correlates with the velocity of the tornado. The tower was analyzed under high-intensity wind loads until brittle failure occurred at scale 8. This result indicates that the wind velocity exceeded 83.38 m/sec, aligning with the results obtained from the SAP2000 software.

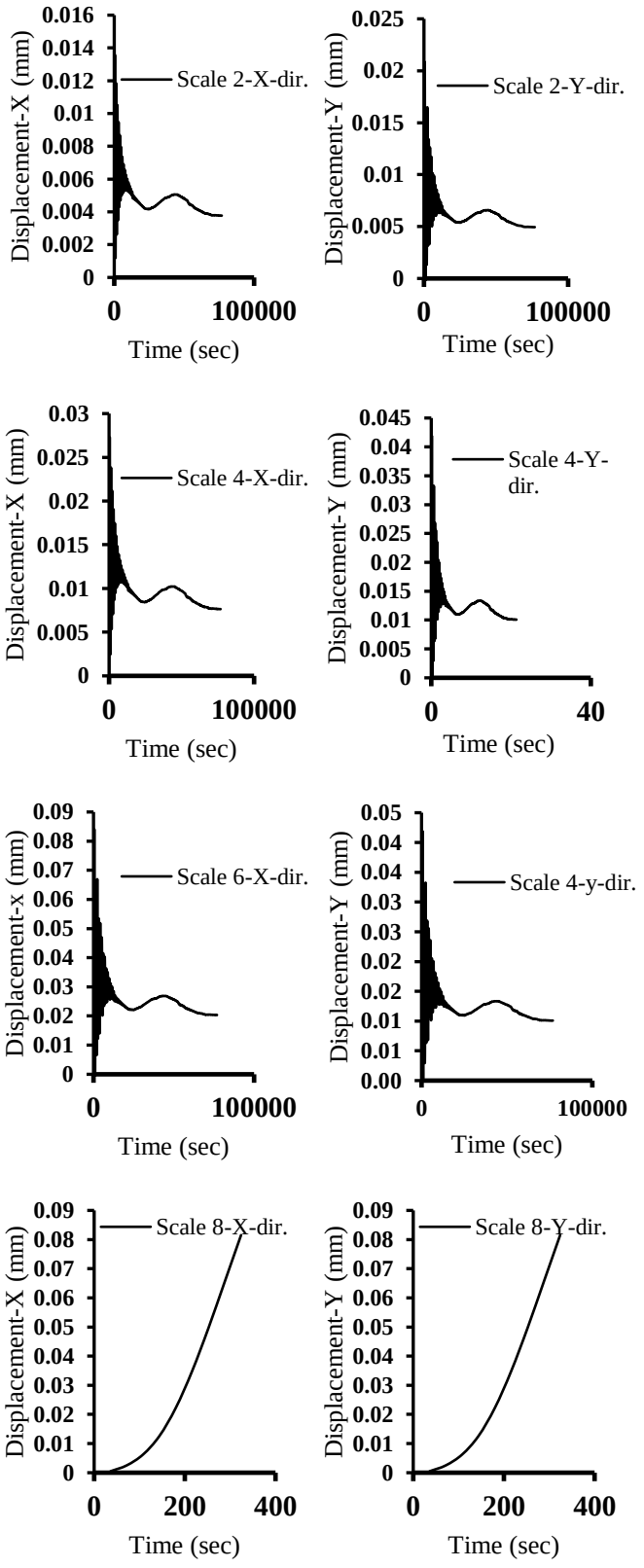

Figure 18. Displacement histories in X and Y-direction of the tower under the scaled wind intensity measure.

4.7.2. Results of Inter-Story Tower Drift

Fig. 19 shows the story drift of the lattice tower under the records of the wind time histories that are scaled using an intensity measure. The results indicate that the tower behaves in a ductile manner until failure at scale 8 of the tornado loads, due to the nonlinear behavior of the section with fibers, in contrast to the results of SAP2000, which modeled the tower as inelastic sections.

4.7.3. Performance Level of the Tower under Incremental Dynamic Analysis

The study evaluated the performance of a tower with nonlinear material properties and geometry under Incremental Dynamic Analysis (IDA). The IDA curves were generated using results from the OpenSees software. These curves illustrate the relationship between the damage measure (DM). The study defined the maximum peak inter-story drift, on the x-axis, and the intensity measurement (IM), represented as the wind velocity percentage of the estimated high-intensity velocity, on the y-axis. The occurrence of collapse under different levels of tornado wind loads was determined from the dynamic analysis results, indicating excessive lateral displacements (lateral dynamic instability). Fig. 20 displays the IDA curves corresponding to various levels of tornado wind loads. By using FEMA-350 [24], the performance level reflects the collapse prevention for scale 8 of the tornado loads. The use of FEMA-based drift limits and IDA-type approaches was not intended to equate wind and seismic behavior, but rather to provide a structured and transparent framework for evaluating limit-state exceedance under increasing wind intensity. The limitations of this analogy have taken care to apply it within a clearly defined context, ensuring that the physical interpretation aligns with wind-specific behavior.

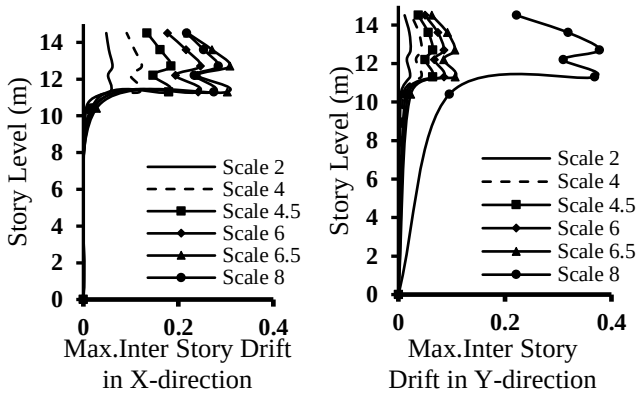

Figure 19. Tower Drift in the X and Y– direction of the models under the scaled wind pressure.

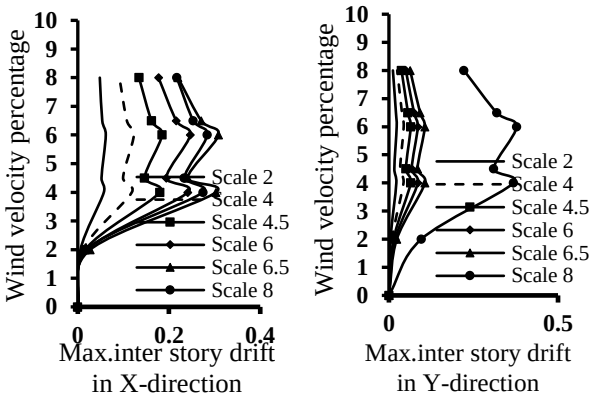

Figure 20. IDA curve of X and Y-directions.

4.8. Cumulative Distribution Function (Collapse Fragility Curve)

A fragility curve is a mathematical tool used to establish the damage level that the tower is likely to exceed under different intensities of ground motions. The primary components of this function are specified by the peak ground acceleration (PGA) and the spectral acceleration (SA). Additionally, the fragility curve is used to estimate the vulnerability regions of the structures under seismic risk analysis. In this study, the fragility curve was applied under various wind load intensities. Fig. 21 illustrates examples of fragility curves (FCs) that indicate the varying probabilities of damage states: slight damage (SD), moderate damage (MD), extensive damage (ED), and complete damage (CD) corresponding to three levels of spectral response.

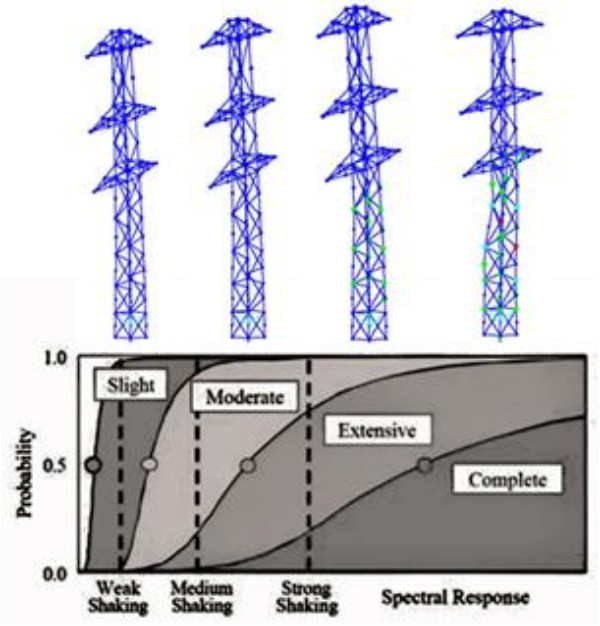

Figure 21. FCs with varying probabilities.

Five performance level (operational phase [OP], immediate occupancy [IO], damage control [DC], life safety [LS], and collapse prevention [CP]) with different probabilities of exceedance (0.5%, 1.0%, 1.5%, 2.0%, and 2.5%) to evaluate the building's wind were adopted to define the limit state [26]. By using MATLAB, the cumulative distribution function (fragility curve) was produced from the results of IDA curves. It relates the ground motion intensity to the probability of collapse [27]. A fragility curve was created in this study to describe the intensity of wind pressure. A lognormal cumulative distribution function is often used to define a fragility function, as per (22).

$$P(C \mid IM = x) = \Phi\left(\frac{\ln(x/\theta)}{\beta}\right) \quad (22)$$

where $P(C \mid IM = x)$ denotes the wind pressure possibility that a wind pressure with IM = x will expose the structure to collapse, (Φ) is the standard normal cumulative distribution function (CDF), is the median of the fragility function (the IM level with 50% probability of collapse) and is the standard deviation of ln IM (sometimes referred to as the dispersion of IM).

Fragility function parameters can be calculated from the data of the wind load pressure applied to the tower, using scale logarithms as an IM value associated with the onset of collapse, and computing their mean and standard deviation [27].

$$\ln \hat{\theta} = \frac{1}{n}\sum_{i=1}^{n} \ln IM_i \quad (23)$$

$$\hat{\beta} = \sqrt{\frac{1}{n-1}\sum_{i=1}^{n} \left(\ln\left(IM_i/\hat{\theta}\right)\right)^2} \quad (24)$$

Where n reflects the wind pressure number, and IMi is the IM value associated with the onset of collapse for the ith wind pressure.

Fig. 22 illustrates the fragility curve derived from IDA curves. According to the figure below, the tower can be operated up to 0.4% of the wind pressure, as the probability of damage at the operational phase (OP) stage is 70%. In the other case, at 0.5 percent of the actual wind pressure, the probability of achieving the IO performance level is 70.7%. This indicates that the tower may experience some damage in these locations. However, for the strong scale of the wind pressure which represents the highest level of performance that the tower can achieve, with one scale wind pressure that reflects the scale 4 of the wind pressure, the tower found that there is a 96.3% exceeding the CP level, this reflects that the tower elements with its connections are significantly deteriorating and the tower may be at collapse. Table 5 explains the output fragility curves generated from the IDA curves.

Table 5. Fragility Curves Output.

Pressure scale	OP	IO	DC	LS	CP
0.00	0.000	0.000	0.000	0.000	0.000
1.10	0.000	0.000	0.000	0.001	0.003
1.15	0.000	0.000	0.000	0.003	0.007
1.20	0.000	0.000	0.002	0.007	0.013
1.25	0.000	0.000	0.007	0.016	0.025
1.30	0.000	0.006	0.022	0.034	0.043
1.35	0.017	0.047	0.061	0.068	0.072
1.40	0.700	0.194	0.140	0.122	0.113
1.45	0.999	0.480	0.269	0.200	0.168
1.50	1.000	0.776	0.440	0.303	0.238
1.55	1.000	0.942	0.624	0.425	0.322
1.60	1.000	0.991	0.782	0.554	0.416
1.65	1.000	0.999	0.894	0.678	0.515
1.70	1.000	1.000	0.956	0.784	0.614
1.75	1.000	1.000	0.985	0.867	0.705
1.80	1.000	1.000	0.996	0.925	0.785
1.85	1.000	1.000	0.999	0.961	0.851
1.90	1.000	1.000	1.000	0.982	0.902
1.95	1.000	1.000	1.000	0.992	0.938
2.00	1.000	1.000	1.000	0.997	0.963
4.00	1.000	1.000	1.000	1.000	1.000
6.00	1.000	1.000	1.000	1.000	1.000

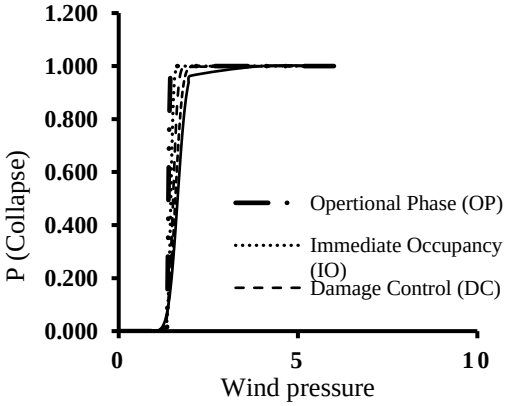

Figure 22. Fragility curve.

5. Conclusions

The study evaluated the high-intensity wind velocity in Al-Kahala, Missan city, Iraq, in 2016 by analyzing an existing steel lattice tower that failed during a tornado. The following conclusions were observed:

1. All towers in Iraq adhere to the design, with the wind velocity risk level in the region being 39 m/sec. Furthermore, the most recent development code for minimum design loads for buildings and other structures suggests that the maximum wind velocity in the study area is 42 m/sec. However, the performance data of the tower indicates that the high-intensity wind velocity exceeded 42 m/sec.

2. The wind risk zone in Missan City lies within an area of zones where the wind velocities barely meet or slightly exceed the criteria specified in a recent design code for minimum design loads for buildings and other structures in Iraq. The wind velocity ranges between 83.38 m/sec-104.22 m/sec, with transmission tower failure at scale 8 till scale 10 for the PBWD approach, and by using the PBFD approach, which is a more conservative estimation, ranges between 83.38 m/sec-104.22 m/sec, with transmission tower failure at scale 8 till scale 10 for the PBWD approach. By using the PBFD approach, which is a more conservative estimation, it could be at wind velocity from scale 6 to scale 8.

3. The structural design of the lattice steel towers constructed in Iraq did not include two very important structural considerations: high-intensity wind load and failure containment.

4. When a Fourier transform is carried out on the time history record of wind velocity, then into frequency components, it can be seen that excitation by wind is mostly governed by low-frequency components within a range between 0 and 2 Hz. This happens to be much lower than the natural frequencies of the structure; hence, resonance cannot take place under the present conditions of wind loading.

5. At scale two of the wind pressure, there was a 96.3% probability that it would exceed the CP level. This means that, in terms of collapse prevention, the tower was found to be susceptible to collapse. Nonlinear analysis recommended implementing and optimizing structural strengthening measures for transmission towers located in high-wind zones of Iraq. Cross-sectional properties and critical connection area enhancements, and a frequency tuning strategy application aimed at reducing possible dynamic amplification due to wind loading, can be considered as structural strengthening measures.

Acknowledgement

The authors thank Prof. Arun Menon, Department of Civil Engineering, Indian Institute of Technology Madras, India, for his useful comments in enhancing the present work. The authors are greatly indebted to Prof. Thaer O. Roomi, Dept. Atmospheric Sciences, Mustansiriyah University, Iraq, who helped in collecting wind speed data used for computations in this paper. Thanks are due to the Indian Institute of Technology Madras (IITM), India, and Mustansiriyah University (www.uomustansiriyah.edu.iq), Baghdad, Iraq, for their help in this research work.

Conflict of Interest

The authors declare no conflict of interest. No conflicts of interest exist, according to the authors, with the publishing of this work.

Author Contribution Statement

All authors conducted the work equally.

References

[1] M. Abdulaqder, M. Kamiran, and Ö. Mustafa, "Comparison of various bracing systems for self-supporting steel lattice structure towers," *Amer. J. Civ. Eng.*, vol. 5, no. 2, pp. 60–68, 2017. doi: https://doi.org/10.11648/j.ajce.20170502.11

[2] D. Nezamolmolki and A. Shooshtari, "Dynamic behavior of lattice transmission towers," *presented at the 10th Int. Congr. Civ. Eng*., Univ. Tabriz, Tabriz, Iran, May 5-7, 2015. [Online]. Available: https://civilica.com/doc/364692/

[3] N. Rao, G. Knight, N. Lakshmanan, and R. I. Nagesh, "Investigation of transmission line tower failures," *Eng. Fail. Anal*., vol. 17, no. 5, pp. 1127–1141, 2010. doi: https://doi.org/10.1016/j.engfailanal.2010.01.008

[4] A. Mills, R. Wiser, and K. Porter, "The Cost of Transmission for Wind Energy in the United States: a Review of Transmission Planning Studies," *Renewable and Sustainable Energy Reviews*, vol. 16, no. 1, pp. 1–19, Jan. 2012, doi: https://doi.org/10.1016/j.rser.2011.07.131

[5] W. Zhang, C. S. Cai, and F. Pan, "Fatigue reliability assessment for long span bridges under combined dynamic loads from winds and vehicles," *Journal of Bridge Engineering*, vol. 18, no. 8, pp. 735–747, 2013. doi: https://doi.org/10.1061/(ASCE)BE.1943-5592.0000411

[6] M. Demircan, Ö. Demir, H. Atay, B. Yazici, O. Eskioğlu, A. Tuvan, and A. Akçakaya, "Climate change projections for Turkey *with new scenarios," presented at The Climate Change and Climate Dynamics Conf.*, Istanbul, Turkey, Oct. 8–10, 2014. doi: http://dx.doi.org/10.13140/2.1.2339.5843

[7] American Society of Civil Engineers (ASCE), "Guidelines for electrical transmission line structural loading, " 4th ed., *ASCE Manuals Rep. Eng. Pract*. No. 74, Amer. Soc. Civ. Eng., 2020. doi: https://doi.org/10.1061/9780784415566

[8] F. C. Macedo, F. Alminhana, L. F. F. Miguel, and A. T. Beck, "Performance-based reliability assessment of transmission lines under tornado actions," *Rel. Eng. Syst. Saf*., vol. 252, p. 110475, 2024. doi: https://doi.org/10.1016/j.ress.2024.110475

[9] H. Gamal, B. Tork, and S. H. El-Beshlawy, "Capacity of transmission tower under wind loading using nonlinear pushover and dynamic analysis," *Al-Azhar Univ. Civ. Eng. Res. Mag. (CERM*), vol. 39, no. 1, pp. 355–365, 2017. [Online]. Available:

https://www.azharcermjournal.com/CERMF1701/P17-01-25.pdf

[10] G.H. Mahmoud, B. S. Tork, and S.A. EL-Beshlawy, "Structural capacity and failure mechanisms of transmission towers under high intensity wind loading," *IOSR J. Mech. Civ. Eng*., vol. 13, no. 5, pp. 25–33, 2016. doi: https://doi.org/10.9790/1684-1305082533

[11] S. Salaam, N. Rao, and P. Raju, "Failure analysis of transmission line tower subjected to combined wind and dust loads," *Curr. Sci.*, vol. 121, no. 4, pp. 511–520, 2021. [Online]. Available: https://www.jstor.org/stable/27310638

[12] W. Zhang, J. Zhu, H. Liu, and H. Niu, "Probabilistic capacity assessment of lattice transmission towers under strong wind," *Front. Built Environ*., vol. 1, no. 20, 2015. doi: https://doi.org/10.3389/fbuil.2015.00020

[13] X. Fu and H. Li, "Rain load for transmission tower-line system," *9th Asia-Pac. Conf. Wind Eng., Auckland, New Zealan*d, 2017. [Online]. Available: https://doi.org/10.17608/k6.auckland.5630578

[14] H. Alinejad, S. Y. Jeong, and T. H.-K. Kang, "Performance-based design of tall buildings for wind load and application of response modification factor," *Wind Struct.*, vol. 31, no. 2, pp. 153–164, 2020. doi: https://doi.org/10.12989/was.2020.31.2.153

[15] American Society of Civil Engineers (ASCE), "Minimum design loads and associated criteria for buildings and other structures, " *ASCE/SEI Standard* 7-22, Amer. Soc. Civ. Eng., 2022. doi: https://doi.org/10.1061/9780784415788

[16] T. T. Fujita and A. D. Pearson, "Results of FPP classification of 1971 and 1972 tornadoes," in Proc. 8th Conf. Severe Local Storms, Denver, American Meteorological Society, Boston, USA, 1973, pp. 142–145. [Online]. Available: http://hdl.handle.net/10605/261906

[17] M. Hooshmand, H. H. Kazemi, and S. A. Zareei, "Evaluation of dynamic analysis of diagrid tall steel building subjected to wind with control approach of operation and acceleration criteria," *Struct. Design Tall Spec. Build.*, vol. 31, no. 2, p. e1902, 2022. doi: https://doi.org/10.1002/tal.1902

[18] T. O.Roomi and F.S. Basheer, "The Synoptic Characteristics, Causes, and Mechanisms of Kahlaa Tornado in Iraq on 14th April 2016," *Baghdad Sci. J.*, vol. 18, no. 2, pp. 1038–1047, 2021.doi: https://doi.org/10.21123/bsj.2021.18.2(Suppl.).1038

[19] The MathWorks, Inc., MATLAB, ver. 9.13.0 (R2022b), Natick, MA, USA, 2022. [Online]. Available: https://www.mathworks.com

[20] Computers and Structures, Inc., SAP2000, ver. 26.1, Berkeley, CA, USA, 2024.

[21] OpenSees, ver. 3.7.1, Pacific Earthq. Eng. Res. Center, Univ. California, Berkeley, CA, USA, 2025. [Online]. Available: http://opensees.berkeley.edu

[22] American Society of Civil Engineers (ASCE), "Seismic evaluation and retrofit of existing buildings, " *ASCE/SEI Standard 41-23, Amer. Soc. Civ. Eng*., 2023. doi: https://doi.org/10.1061/9780784416112

[23] M. S. Rechtman and J. G. S. Silva, "Structural analysis of latticed steel transmission towers subjected to nondeterministic wind loads," *Eng., Technol. Appl. Sci. Res*., vol. 14, no. 6, pp. 18048–18054, 2024. doi: https://doi.org/10.48084/etasr.8990

[24] FEMA, "Recommended seismic design criteria for new steel moment-frame buildings, " FEMA 350, *Fed. Emergency Manag. Agency*, Washington, DC, USA, 2000. [Online]. Available: www.fema.gov

[25] H. A. Abass and H. K. Jarallah, "Plastic hinge zone effect on seismic evaluation of rc frame under Iraqi seismic code loading," *in Proc. 3rd 2021 International Conference on Advances of Sustainable Engineering and its Application (ICASEA 2021)*, Wasit, Iraq, 2021, pp. 159–164. doi: https://doi.org/10.1109/ICASEA53739.2021.9733091

[26] H. K. Jarallah, D. K. Paul, and Y. Singh, "Seismic evaluation and retrofit on an existing hospital building," *J. Eng. Sustain. Dev*., vol. 24, no. 6, pp. 1–21, 2020. doi: https://doi.org/10.31272/jeasd.24.6

[27] H.-N. Li, R.-H. Li, C. Li, and D.-B. Wang, "Development of hysteretic model with dynamic effect and deterioration for seismic-performance analysis of reinforced concrete structures," J. Struct. Eng., vol. 146, no. 10, 2020.doi: https://doi.org/10.1061/(ASCE)ST.1943-541X.0002774